Effect of Mn and V on structure and mechanical properties of high-entropy alloys based on CoCrFeNi system

G.A. Salishchev [a], M.A. Tikhonovsky [b], D.G. Shaysultanov [a], N.D. Stepanov [a,*], A.V. Kuznetsov [a], I.V. Kolodiy [b], A.S. Tortika [b], O.N. Senkov [c]

[a] *Laboratory of Bulk Nanostructured Materials, Belgorod State University, Belgorod 308015, Russia*
[b] *National Science Center "Kharkov Institute of Physics and Technology" NAS of Ukraine, Kharkov 61108, Ukraine*
[c] *UES, Inc., 4401 Dayton-Xenia Rd., Dayton, OH 45432, USA*

ARTICLE INFO

ABSTRACT

Microstructure and mechanical properties of equimolar composition alloys FeCrCoNi, FeCrCoNiV, FeCrCoNiMn and FeCrCoNiMnV were studied in as-solidified and annealed conditions. The FeCrCoNi and FeCrCoNiMn alloys were single-phase FCC solid-solutions in both conditions. However, the FeCrCoNiV and FeCrCoNiMnV alloys consisted of the intermetallic σ-phase matrix with a tetragonal crystal lattice and precipitates of a disordered FCC phase. The crystal structures of these alloys were found to be not affected by annealing. A number of criteria were considered to explain phase composition of the studied alloys. It was shown that poor compatibility of V with other alloying elements caused significant distortions of FCC solid solution and thus promoted formation of the σ phase. Tensile and compressive properties of these alloys together with their microhardness were determined. Significant strengthening accompanied by the loss of ductility due to formation of the σ phase was demonstrated in the V containing alloys. The characteristics of the microstructure formation in the studied alloys were discussed.

1. Introduction

The concept of high entropy alloys (HEAs) is one of the most recent developments in material science [1]. Depending on their composition and microstructure, HEAs can offer diverse range of attractive properties, such as high hardness and wear resistance [2], exceptional high temperature strength [3,4], good low-temperature ductility [5,6], and superplastic behavior [7,8]. HEAs are defined as alloys consisting of 5 or more principal elements with nearly equimolar fractions [1]. High entropy of mixing is thought to prevent formation of intermetallic phases. Thus, the alloys should consist mainly from simple solid solutions. However, there are experimental evidences that ordered solid solutions and/or intermetallic phases may also exist in many HEAs [9,10]. This indicates that the high entropy of mixing of the alloying elements is not sufficient to prevent formation of intermetallic phases in favor of solid solution phases in HEAs [11].

Hume-Rothery rules are generally used to predict formation of continuous solid solutions in conventional metallic alloys. For the formation of continuous solid solution of two elements, the following requirements should be met: (i) the difference between the atomic radii of the alloying elements [$(r_{solute} - r_{solvent})/r_{solvent}$] $\times$ 100%] is less than 15%; (ii) the crystal structures of the elements are identical; (iii) the elements have the same valence electron concentration (VEC); (iv) the electronegativities of the elements are similar [12]. However, it is not clear whether such rules can be applied directly to the multicomponent HEAs, as it is hard to expect that all of the alloying elements have, for example, the same crystal structure and VEC. A number of attempts have been made [13–16] to develop some criteria based on Hume-Rothery rules which could be used to predict formation of solid solution or intermetallic phases in HEAs. However, strict methodology has not been developed yet.

It is known that several 4-component equiatomic alloys, such as WNbMoTa [17] or CoCrFeNi [18–20] exhibit simple solid solution single phase structures. Increasing the number of alloying elements generally causes phase separation, in spite of an increase in ΔS_{mix}. For example, a complex multiphase structure is formed in the CoCrFeNi–Al system [21]. In contrast, in the CoCrFeNiMn alloy the presence of only simple solid solution is confirmed by a number of investigations [11,22]. Such different behavior can be expected, as Mn is closer (than Al) to the other components of the alloy to fulfill Hume-Rothery rules. Another "neighbor" of the elements of the CoCrFeNi alloy in the periodic table is V. We did not find any information in the literature on the alloys with

* Corresponding author. Address: Laboratory of Bulk Nanostructured Materials, Belgorod State University, Pobeda 85, Belgorod 803015, Russia. Tel.: +7 4722 585416.
    E-mail addresses: stepanov@bsu.edu.ru, stepanov.nikita@icloud.com (N.D. Stepanov).

compositions close to CoCrFeNiV and CoCrFeMnNiV. However, complex structures containing intermetallic phases, including the σ phase, were reported for the $Al_{0.5}CoCrCuFeNiV_x$ alloy system [23]. The σ phase was also found in the alloys such as CoFeMnNiV and CoCrMnNiV [11]. However, the presence of such elements as Al, Cu and Mn or the absence of Cr or Fe makes it impossible to clearly denote the effect of V on the microstructure formation of the CoCrFeNi-based alloys. One should also note that systematic investigations of the effect of alloying of the CoCrFeNi-based alloys with Mn and V on tensile properties have not been performed.

In this work, the microstructure and mechanical properties of the CoCrFeNi, CoCrFeNiMn, CoCrFeNiV and CoCrFeNiMnV HEAs are reported, both in as-solidified and annealed conditions. Mn and V were chosen as the alloying elements as they are "neighbors" of the elements of the base alloy in the periodic table and thus are likely to form simple solid solutions. The following goals were pursued: (i) to investigate the effects of alloying with V alone or together with Mn on the microstructure of CoCrFeNi alloy; (ii) to provide additional information on usefulness of the Hume-Rothery based criteria for the prediction of the crystal structures in HEAs; and (iii) to evaluate mechanical properties of the $CoCrFeNiMn_xV_y$ alloys and their interplay with the microstructure.

2. Experimental procedures

Equiatomic alloys with the compositions of CoCrFeNi, CoCrFeNiMn, CoCrFeNiV and CoCrFeNiMnV were produced by arc melting of the components in high-purity argon inside a water-cooled copper cavity. The purities of the alloying elements were above 99.9%. To ensure chemical homogeneity, the ingots were flipped over and re-melted a least 5 times. The produced ingots had dimensions of about $6 \times 15 \times 60$ mm³. The alloys were studied both in as-solidified state and after homogenization annealing. Homogenization was carried out at 1000 °C for 24 h, in accord to previous work by Gali and George [5] who used these conditions to homogenize the CoCrFeNi, CoCrFeNiMn alloys. Prior to homogenization, the samples were sealed in vacuumed (10^{-2} torr) quartz tubes filled with titanium chips to prevent oxidation. After annealing, the tubes were removed from the furnace and the samples were cooled inside the vacuumed tubes down to room temperature due to heat exchange with surrounding air.

Microstructure of the alloys was studied using X-ray diffraction (XRD), and scanning (SEM) and transmission (TEM) electron microscopy. XRD analysis was performed using RIGAKU diffractometer and Cu Kα radiation. Samples for SEM observations were prepared by careful mechanical polishing. SEM investigations were performed utilizing Quanta 200 3D microscope equipped with energy-dispersive (EDS) detector. Samples for TEM analysis were prepared by conventional twin-jet electro-polishing of mechanically pre-thinned to 100 μm foils, in a mixture of 95% C_2H_5OH and 5% $HClO_4$ at the 27 V potential. TEM investigations were performed using JEOL JEM-2100 apparatus equipped with EDS detector at accelerating voltage of 200 kV.

Vickers microhardness, HV, was measured on polished cross-section surfaces using a 136 Vickers diamond pyramid under a 250 g load applied for 15 s. For microhardness measurements of individual phases, 10 g load was applied. Tensile testing was preformed utilizing Instron 5882 machine. Specimens had gauge dimensions of $5 \times 3 \times 1.5$ mm³. Initial strain rate was 10^{-3} s⁻¹. Three tensile specimens were tested for each condition. The similar tests provided maximum scatters of ~5% in the yield strength and tensile strength and ~10% in tensile ductility. Compressive tests were performed on rectangular specimens with dimensions of $7 \times 5 \times 5$ mm³ using the same machine. One compression sample was tested for each condition. The initial strain rate was 10^{-3} s⁻¹.

3. Results

3.1. As-solidified condition

XRD patterns of the as-solidified alloys are shown in Fig. 1. The pattern of the base CoCrFeNi alloy demonstrates the presence of a single phase with the FCC lattice (a = 3.577 Å). Only one FCC phase, with a slightly higher lattice parameter (a = 3.602 Å) is also found in the CoCrFeNiMn alloy. The XRD pattern from this alloy shows only two peaks, (200) and (400), which is an indication of the formation of very large grains in this alloy after solidification. Addition of V, both to the base- and to the Mn-containing alloys,
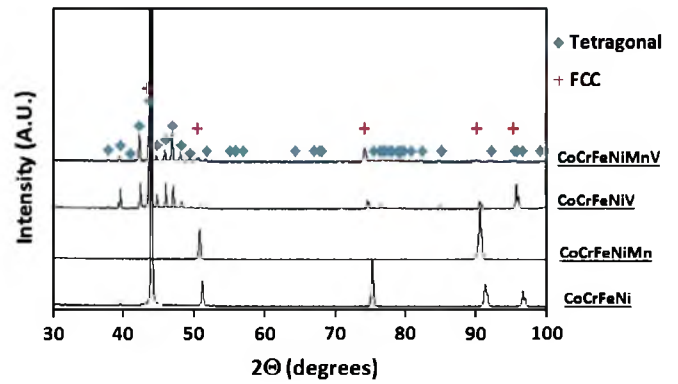

Fig. 1. X-ray diffraction patterns of the studied alloys in as-solidified condition.

causes formation of the σ phase with a tetragonal structure. The σ phase has the lattice parameters of a = 8.794 Å, c = 4.566 Å for the CoCrFeNiV alloy and a = 8.826 Å, c = 4.578 Å for the CoCrFeNiMnV alloy. A disordered FCC phase is also found in these alloys. The lattice parameter of this phase is a = 3.593 Å for CoCrFeNiV and a = 3.612 Å for CoCrFeNiMnV.

The microstructures of the as-solidified alloys are shown in Fig. 2. The base CoCrFeNi alloy has a single-phase structure consisting of slightly elongated, from bottom to top of the ingot, grains with the average width of about 100–150 μm and average length of 200–300 μm (Fig. 2a). The measured compositions of grains are reasonably close to the nominal composition of the alloy (Table 1). The CoCrFeNiMn alloy has a dendritic microstructure (Fig. 2b); the dendrite areas (light-grey ones, point 1) are slightly enriched with Co, Cr and Fe (Table 1) and contain about 16.4–16.7% of Ni and Mn. Contrary, inter-dendritic areas (dark-grey ones, point 2) are enriched with Ni and Mn and contain about 16.7–17.0% of each of the remaining elements. The grain size is estimated to be larger 300–400 μm, and only one grain is shown in Fig. 2b. The CoCrFeNiV alloy has a complex microstructure (Fig. 2c) composed from grain boundary phase (point 1), enriched with Ni and depleted of Cr (Table 1), and grain interiors (point 2), slightly enriches with Cr and depleted of Ni. The average size of the grains (measured as the average distance between grain boundary phase particles) is about 30 μm. The grain interior consists of two phases with very fine scale (shown in a higher magnification insert): dark matrix and light elongated particles. This type of microstructure generally occurs after eutectoid transformation. The microstructure of the CoCrFeNiMnV alloy (Fig. 2d) is similar to the CoCrFeNiV alloy. The grain boundary phase is enriched with Ni and Mn, and grain interiors are slightly enriched with Cr and V (Table 1). The difference between the microstructures of the CoCrFeNiV and CoCrFeNiMnV alloys is found inside the grain interiors (shown in a higher magnification insert): the second-phase particles have more equiaxed shape and are coarser in the alloy with Mn. The grain size in the CoCrFeNiMnV alloy is about 20 μm.

Additional information about the microstructure of the alloys was obtained from TEM investigations (Fig. 3). TEM confirms that the base CoCrFeNi alloy has a single-phase FCC crystal structure (Fig. 3a) and all grains have nearly nominal chemical composition (Table 2). At the same time, slight variations of the chemical composition of the FCC phase are found in the CoCrFeNiMn alloy (Table 2); the chemical compositions of the dendrite and interdendrite areas were determined to be similar to those determined by SEM-EDS. Fig. 3c and d demonstrate grain interiors of the CoCrFeNiV and CoCrFeNiMnV alloys. Both of them have similar features. The matrix phase has a tetragonal structure and thus is identified as a σ phase. It is enriched with Cr and V, and depleted of Ni
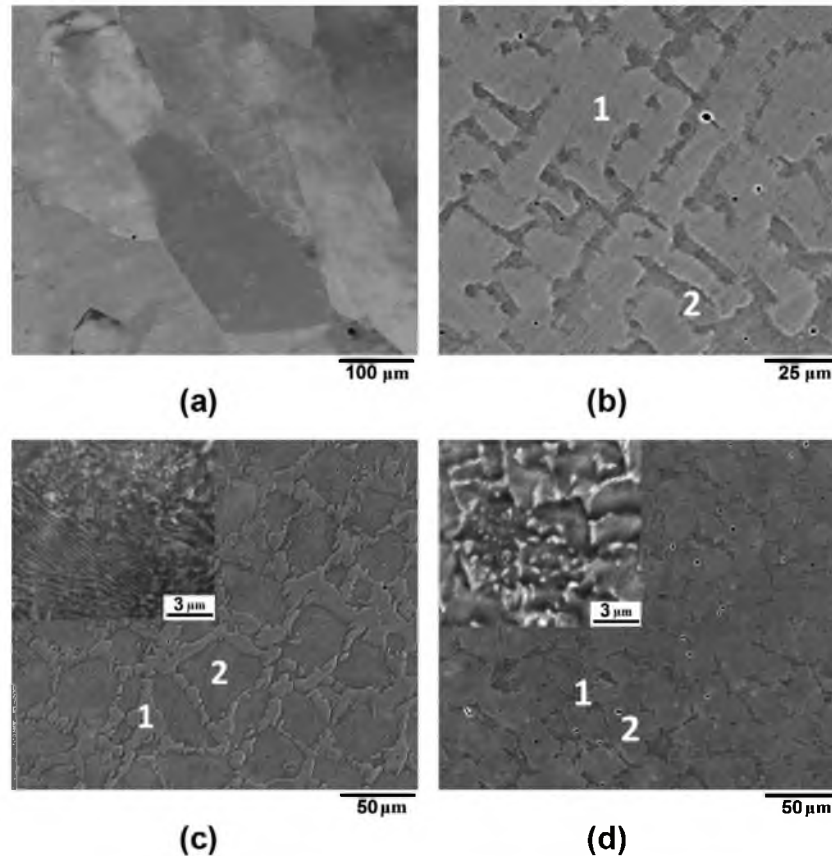
Fig. 2. Backscatter electron (BSE) images of the microstructure of the studied alloys in the as-solidified condition: (a) CoCrFeNi, (b) CoCrFeNiMn, (c) CoCrFeNiV, and (d) CoCrFeNiMnV. Different structural constituents are identified with numbers and their compositions are given in Table 1.

Table 1
Chemical composition of the alloy constituents (as shown in Fig. 2) in the as-solidified condition. The data derived by SEM-based EDS.

Element, at.%		Co	Cr	Fe	Ni	Mn	V
CoCrFeNi							
1	Grains	24.7	25.3	25.2	24.8	–	–
CoCrFeNiMn							
1	Dendrites	21.0	21.8	22.1	16.7	16.4	–
2	Interdendrites	16.8	17.0	16.7	22.9	26.6	–
CoCrFeNiV							
1	Grain boundary phase	20.9	17.0	19.4	24.4	–	18.3
2	Grain interiors	18.9	22.1	20.0	17.8	–	21.2
CoCrFeNiMnV							
1	Grain boundary phase	16.1	12.6	15.5	22.7	19.1	14.0
2	Grain interiors	16.3	18.0	17.4	15.6	15.5	17.2

(and Mn in the alloy containing Mn). Inside the matrix, elongated particles with the FCC structure are found. These particles are depleted of Cr and V and enriched with Ni (and also Mn, in the alloy containing Mn).

3.2. Annealed condition

The XRD patterns of the annealed alloys are shown in Fig. 4. No significant changes are found relative to the as-solidified condition (Fig. 1). The annealed CoCrFeNi and CoCrFeNiMn alloys consist of a single FCC phase. The annealed CoCrFeNiV and CoCrFeNiMnV alloys consist of two phases, σ and FCC. However, the lattice parameters of the existing phases change after

annealing. The FCC phase has the lattice parameter of $a = 3.568$ Å, $a = 3.595$ Å, $a = 3.595$ Å and $a = 3.610$ Å for the CoCrFeNi, CoCrFeNiMn, CoCrFeNiV and CoCrFeNiMnV alloys respectively. The tetragonal σ phase has the lattice parameters of $a = 8.823$ Å and $c = 4.577$ Å in the CoCrFeNiV alloy and $a = 8.290$ Å and $c = 4.576$ Å in the CoCrFeNiMnV alloy.

After annealing, grains become more equiaxed, with the average grain size of about 200 μm, in the CoCrFeNi alloy (Fig. 5a). At the same time, annealing of the CoCrFeNiMn alloy causes transformation of the dendritic microstructure into a granular one, with the average grain size of ~130 μm (Fig. 5b). The chemical composition of the grains now corresponds to the nominal chemical composition of the alloy (Table 3). The annealed CoCrFeNiV alloy (Fig. 5c) consists of two phases: a dark σ-phase matrix is enriched with Cr and V and depleted of Ni and bright second-phase particles are enriched with Ni and depleted of V and Cr (Table 3). Two different morphologies of the particles can be distinguished: coarse particles with irregular shape, most likely originated from the grain boundary phase present in the as-solidified condition, and relatively fine, round-shaped particles in the core regions. Both types of the particles have the same composition and FCC crystal structure. The development of the grain structure is found in the matrix phase. The microstructure of the CoCrFeNiMnV alloy consists of the σ-phase matrix with the average grain size of 12 μm and FCC particles of two types – coarse ones with a complex shape and fine, reasonably round-shaped ones (Fig. 5d). The matrix is enriched with Cr and V and depleted of Mn and Ni, and the particles are enriched with Ni and Mn and depleted of Cr and V (Table 3). The volume fraction of the second-phase particles is estimated to be ≈41% and ≈27% in the CoCrFeNiV and CoCrFeNiMnV alloys, respectively.

(a)

(b)

(c)

(d)
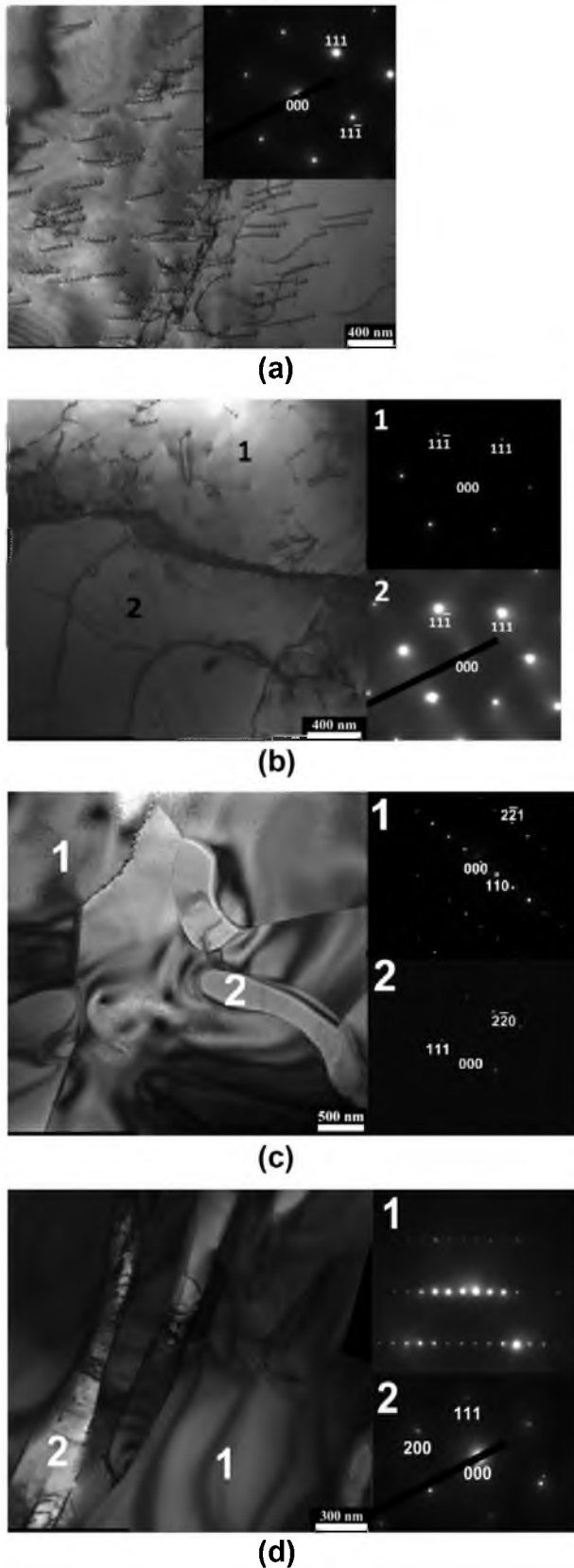
Fig. 3. TEM images of the microstructure of the studied alloys in as-solidified state, selected area diffraction patterns for corresponding phases are provided: (a) CoCrFeNi, (b) CoCrFeNiMn, (c) CoCrFeNiV, and (d) CoCrFeNiMnV. Different structural constituents are identified with numbers and their compositions are given in Table 2.

3.3. Mechanical properties

The results of microhardness measurements are summarized in Table 4. The base CoCrFeNi alloy has microhardness of 160 HV in the as-solidified state. Annealing causes a decrease in the microhardness down to 134 HV. The CoCrFeNiMn alloy has slightly higher microhardness of 170 HV in the as-solidified condition and 135 HV after annealing. Alloying of these two alloys with V has a pronounced effect on microhardness. In the as-solidified condition, the microhardness increases by more than three times, e.g. to 524 HV in CoCrFeNiV and to 650 HV in CoCrFeNiMnV. Annealing results in a further increase in microhardness of CoCrFeNiV to 587 HV. However, microhardness of the CoCrFeNiMnV alloy remains nearly unaffected by annealing, and its value is 636 HV. Additionally, microhardness of the σ phase matrix was measured in the annealed state of the CoCrFeNiV and CoCrFeNiMnV alloys. The σ phase has microhardness of 1002 HV in the CoCrFeNiV alloy and 1025 HV in the CoCrFeNiMnV alloy. Fine scale of the FCC particles prohibited adequate measurements of their microhardness.

The engineering stress – engineering strain tensile curves of the CoCrFeNi, CoCrFeNiMn and CoCrFeNiV alloys in the as-solidified and annealed conditions are given in Fig. 6. The respective tensile properties, such as yield stress ($\sigma_{0.2}$), ultimate tensile strength (σ_u), and elongation to fracture (δ) are given in Table 5. The stress-strain curves of the CoCrFeNi and CoCrFeNiMn alloys, both in as-solidified and annealed states, clearly demonstrate significant capability of strain hardening and thus good overall ductility. The elongation to fracture of the base alloy is 83–87% and that of the CoCrFeNiMn alloy is 68–71%. Slightly lower ductility of the CoCrFeNiMn alloy in comparison with the CoCrFeNi alloy corroborates well with a higher yield strength, because the ultimate tensile strengths and strain hardening coefficients of these alloys are comparable. For example, $\sigma_{0.2}$ equals to 215 MPa for CoCrFeNiMn and 140 MPa for CoCrFeNi in the as-solidified condition, whereas σ_u respectively equals to 491 MPa and 488 MPa. Annealing causes pronounced softening of both alloys. $\sigma_{0.2}$ decreases to 162 MPa in CoCrFeNiMn and to 130 MPa in CoCrFeNi; σ_u decreases respectively to 443 MPa and 458 MPa. The tensile behavior of the CoCrFeNiV alloy is distinctively different from that of the two above-mentioned alloys. This alloy does not exhibit plastic deformation at all, and demonstrates brittle fracture at the stress values of slightly above 300 MPa. Annealing does not have any pronounced effect on tensile behavior of the CoCrFeNiV alloy. Tensile behavior of the CoCrFeNiMnV alloy was similar to the behavior of the CoCrFeNiV alloy. It did not show any plastic deformation and fractured during elastic loading already at stress values of 62–90 MPa. Therefore, the deformation curve for this alloy is not shown in Fig. 6.

In order to obtain additional information on mechanical behavior of the brittle V-containing alloys, compression tests were performed on the specimens in the homogenized condition. The compression engineering stress–engineering strain curves are given in Fig. 7, and compression properties, such as yield stress, $\sigma_{0.2}$, peak stress, σ_p, and compressive strain to fracture, ε, are summarized in Table 6. For the sake of comparison the data on compressive behavior of the base CoCrFeNi alloy is also included. The base CoCrFeNi alloy demonstrates relatively low yield stress of 190 MPa, high ductility and high strain hardening; its strength increases to 1000 MPa and it shows no signs of cracking after compressive deformation of 75%. Alloying with V results in very significant strengthening, $\sigma_{0.2}$ and σ_p are equal to 1435 MPa and 1665 MPa respectively for the CoCrFeNiV alloy. Strengthening is accompanied with the loss in the compression ductility down to 2.5%. An addition of Mn promotes a further increase in strength. In particular, $\sigma_{0.2}$ increases to 1660 MPa and σ_p increases to

Table 2

Chemical composition and the crystal lattice type of the alloy constituents (as shown on Fig. 3) in as-solidified state. The data derived from TEM-based EDS.

Element, at.%			Co	Cr	Fe	Ni	Mn	V
CoCrFeNi								
1	Grains	FCC	25.0	24.6	25.1	25.3	–	–
CoCrFeNiMn								
1	Dendrites	FCC	20.1	22.8	21.7	17.6	17.9	–
2	Interdendrites	FCC	18.3	21.1	18.1	19.1	23.4	–
CoCrFeNiV								
1	Matrix	Tetragonal (D8b)	18.4	24.9	19.1	15.2	–	22.3
2	Particles	FCC	20.7	17.8	21.2	23.1	–	17.2
CoCrFeNiMnV								
1	Matrix	Tetragonal (D8b)	16.3	19.1	15.4	16.2	14.0	18.9
2	Particles	FCC	18.0	14.1	17.3	17.6	19.6	13.4
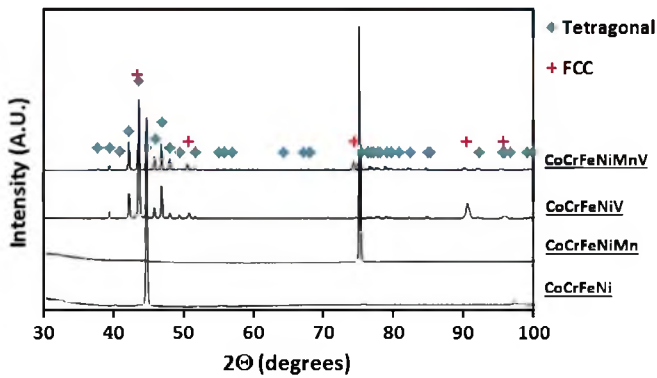
Fig. 4. X-ray diffraction patterns of the studied alloys after homogenization annealing.

1885 MPa in the CoCrFeNiMnV alloy. However, the compression ductility of this alloy is very low, only 0.5%.

4. Discussion

4.1. Microstructure of CoCrFeNiMn$_x$V$_y$ alloys

Microstructural investigations have revealed that the CoCrFeNi and CoCrFeNiMn alloys are single phase FCC solid solutions, in agreement with previous work [4,5,11,22]. While the CoCrFeNi alloy has a simple granular structure, both in as-solidified and homogenized conditions, a dendritic structure was found in the as-solidified state of the CoCrFeNiMn alloy. According to the XRD analysis and TEM data, both dendrite and interdendrite areas have the same FCC lattice. Dendrites are enriched with Co, Cr and Fe, and interdendrite areas are enriched with Mn and Ni. It seems obvious that dendrites are enriched with high melting point elements (T_m equals 1768 K, 2180 K and 1811 K for Co, Cr and Fe respectively) and interdendrites are enriched with elements with lower melting points (1728 K and 1519 K for Ni and Mn respectively). Annealing promotes homogenization of the chemical composition and thus elimination of the dendritic structure. Presence of dendritic segregation in as-solidified state and their elimination after annealing correlates with previous findings by Cantor et al. [22] and Otto et al. [11], respectively.

The microstructure of the CoCrFeNiV and CoCrFeNiMnV alloys is significantly different from those described above. It is more complex and several structural constituents are identified. In the as-solidified state, an eutectoid-like structure inside the grains is distinguished. Grains are separated by thick layers of a secondary phase containing preferably Ni. TEM analysis demonstrated that the eutectoid-like regions are composed mainly from a tetragonal phase enriched with Cr and V, which is identified as a σ phase.

The second component of the eutectoid-like structure is present in the form of particles with the FCC lattice, enriched with Ni. Considering the facts that (i) the FCC particles inside the eutectoid-like structure and the grain boundary phase have almost identical composition and (ii) according to XRD data, only two crystal lattices are present in the alloys, it was suggested that the grain boundary phase also has the FCC structure. The complex structure in the V-containing alloys is a result of solidification and solid-state transformation. The following scenario of the phase transformations in these two alloys is proposed. The first phase to solidify is a high-temperature phase, which is a predecessor of the eutectoid-like structure. Possibly this phase has a BCC structure, like a high-temperature δ ferrite in steels. The second phase to solidify is the FCC phase found at grain boundaries. Upon cooling, the high-temperature BCC phase undergoes eutectoid transformation into a mixture of the σ phase and FCC phase. Similar transformation is observed in duplex steel [24].

Upon annealing, the microstructures of the CoCrFeNiV and CoCrFeNiMnV alloys are significantly changed. The grain boundary particles are retained, however, they do not form nearly continuous network like in as-solidified state but appear as separate coarse particles with a complex shape. The eutectoid-like structure drastically changes after annealing: the σ-phase forms a continuous matrix containing relatively coarse spherical particles of the FCC phase. Most possibly the changes in the eutectoid-like structure after annealing were caused by extensive spheroidization and coagulation of fine, often elongated particles of the FCC phase found in the as-solidified alloys.

To summarize the data on microstructure of the studied alloys, the following conclusions can be made: (i) the CoCrFeNi and CoCrFeNiMn alloys exhibited simple FCC solid solution microstructures; (ii) addition of V to the CoCrFeNi and CoCrFeNiMn alloys causes formation of a complex structure consisting of the σ phase matrix and second-phase FCC particles; (iii) homogenization annealing of the studied alloys did not change the phase compositions but significantly affected the phase morphology.

4.2. Phase stability in CoCrFeNiMn$_x$V$_y$ alloys

High entropy alloys (HEAs) usually consist of 5 or more principal elements with nearly equimolar concentrations and, depending on the choice of the constituent elements; these alloys can be disordered solid solutions or additionally contain intermetallic phases [11,20–22]. It is thought that the high entropy of mixing of the alloying elements $\Delta S_{mix} = -R \sum c_i \ln c_i$, where R is the gas constant and c_i is the atomic fraction of element i, is responsible for the formation of solid solution phases in HEAs [1], as the Gibbs free energy of the disordered phases is considerably reduced by the entropy term, $T\Delta S_{mix}$. However, this is not the case for the studied CoCrFeNiMn$_x$V$_y$ system. Indeed, the four-component CoCrFeNi and
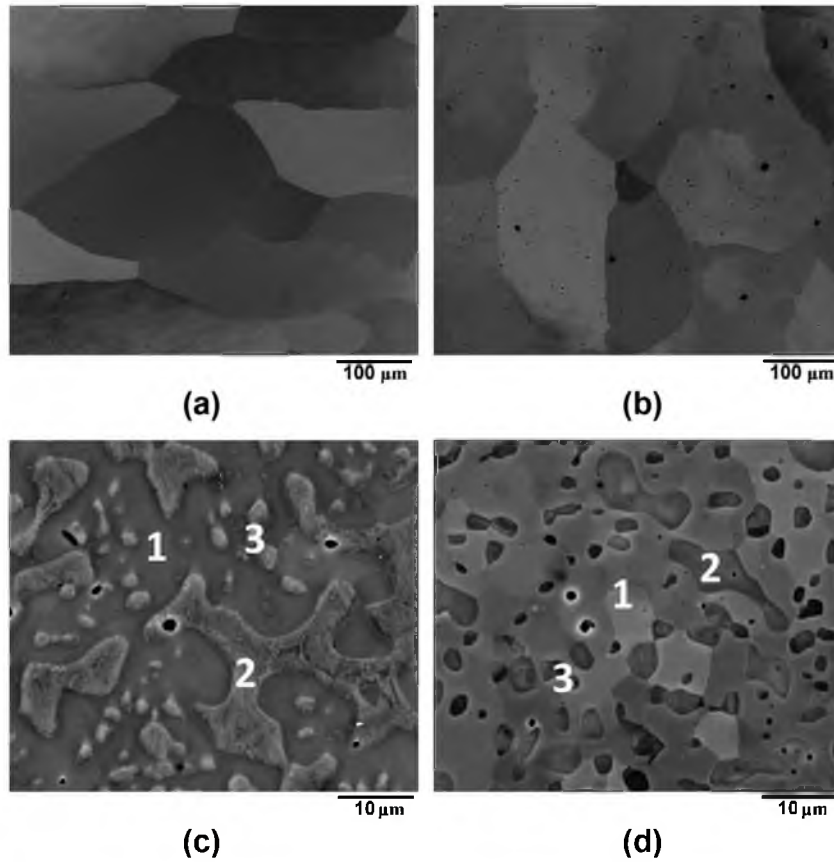
Fig. 5. Backscattered images of microstructure of studied alloys in annealed state: (a) CoCrFeNi, (b) CoCrFeNiMn, (c) CoCrFeNiV, and (d) CoCrFeNiMnV. Different structural constituents are identified with numbers and their compositions are given in Table 3.

Table 3
Chemical composition of alloys' constituents (as shown in Fig. 1) in the annealed condition. The data derived by SEM-based EDS.
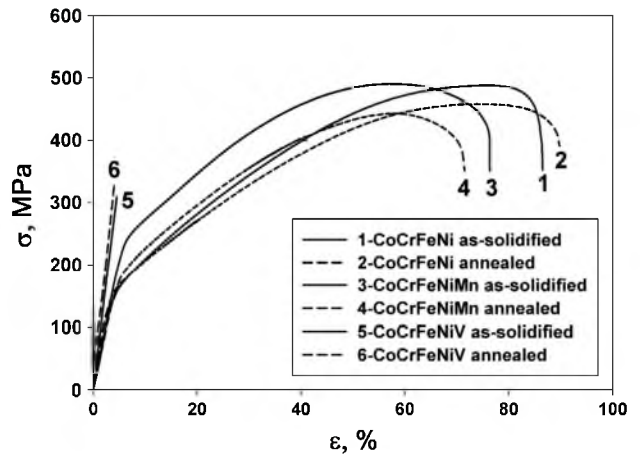
Element, at.%		Co	Cr	Fe	Ni	Mn	V
CoCrFeNi							
1	Grains	25.1	24.5	25.4	25.0	–	–
CoCrFeNiMn							
1	Grains	19.6	20.5	19.9	20.9	19.1	–
CoCrFeNiV							
1	Matrix	19.3	24.1	19.4	15.3	–	21.9
2	Coarse particles	20.6	14.3	20.8	26.4	–	17.4
3	Fine particles	21.1	14.7	20.5	26.8	–	17.3
CoCrFeNiMnV							
1	Matrix	16.7	20.0	16.6	13.5	14.6	18.6
2	Coarse particles	16.9	11.4	17.0	24.6	17.8	12.3
3	Fine particles	17.0	11.7	16.7	24.4	17.8	12.4

Table 4
Microhardness of the studied alloys in as-solidified and annealed states.

Alloy	Microhardness, HV	
	As-solidified	Annealed
CoCrFeNi	160 ± 4	134 ± 4
CoCrFeNiMn	170 ± 4	135 ± 2
CoCrFeNiV	524 ± 15	587 ± 17
CoCrFeNiMnV	650 ± 27	636 ± 23

Fig. 6. Stress–strain curves obtained during tensile testing of CoCrFeNi, CoCrFeNiMn and CoCrFeNiV alloys.

five-component CoCrFeNiMn alloys are single-phase FCC solid solutions and their entropies of mixing are 11.5 J/mole K and 13.4 J/mole K, respectively. On the other hand, the five-component CoCrFeNiV alloy, which has the same ΔS_{mix} = 13.4 J/mole K as

CoCrFeNiMn, and the six-component CoCrFeNiMnV alloy, which has the highest mixing entropy (ΔS_{mix} = 14.9 J/mole K) among the studied alloys, are intermetallic-based alloys consisting of the σ-phase matrix and second-phase FCC particles. Therefore, additional recently proposed criteria [13–16], should be used for predicting solid solution or intermetallic phase formation in the studied HEAs. In accord to Hume-Rothery rules for binary substitutional solid solutions [25], the solvent and solute should have small atomic size difference, the same valence and similar electronegativity. Therefore, it is worth to explore if these rules also work for complex high entropy alloys.

Table 5
Tensile properties of the CoCrFeNi, CoCrFeNiMn and CoCrFeNiV alloys in as-solidified and annealed states.

Alloy	$\sigma_{0.2}$, MPa	σ_u, MPa	δ, %
CoCrFeNi			
As-solidified	140	488	83
Annealed	130	458	87
CoCrFeNiMn			
As-solidified	215	491	71
Annealed	162	443	68
CoCrFeNiV			
As-solidified	–	311[a]	0
Annealed	–	330[a]	0
CoCrFeNiMnV			
As-solidified	–	90[a]	0
Annealed	–	62[a]	0

[a] The CoCrFeNiV and CoCrFeNiMnV alloys exhibited brittle fracture, both in as-solidified and annealed states, and the given values correspond to the fracture strength values.
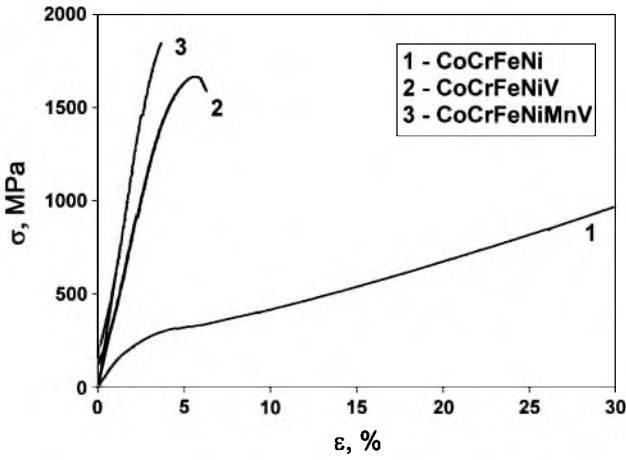
Fig. 7. Stress–strain curves obtained during compressive testing of the CoCrFeNi, CoCrFeNiV and CoCrFeNiMnV alloys in annealed state.

Table 6
Compressive properties of the CoCrFeNi, CoCrFeNiV and CoCrFeNiMnV alloys in annealed state.

Alloy	$\sigma_{0.2}$, MPa	σ_p, MPa	ε, %
CoCrFeNi	190	>1000*	>75*
CoCrFeNiV	1435	1665	2.5
CoCrFeNiMnV	1660	1845	0.5

* The CoCrFeNi alloy exhibited no fracture after strain of 75% and the stress level continuously increased with strain.

Zhang et al. [13] proposed two parameters to predict formation of solid solution and/or intermetallic phases in HEAs. These are the atomic size difference, $\delta r = 100\%\sqrt{\sum c_i(1 - r_i/\bar{r})^2}$, and the enthalpy of mixing, $\Delta H_{mix} = \sum 4\omega_{ij}c_ic_j$. Here c_i and r_i are the atomic fraction and the atomic radius, respectively, of element i, $\bar{r} = \sum c_i r_i$ is the average atomic radius, and ω_{ij} is a concentration-dependent interaction parameter between elements i and j in a sub-regular solid solution model [26]. It was found for a number of HEAs that solid solutions form in HEAs for which $\delta r < 6.2\%$ and ΔH_{mix} is in the range from -20 kJ/mole to 5 kJ/mole, while intermetallic phases can be present in HEAs for which $\delta r > 3\%$ and $\Delta H_{mix} < 5$ kJ/mole [13]. Therefore, the ΔH_{mix} criterion predicts formation of only intermetallic phases in HEAs for which $\Delta H_{mix} < -20$ kJ/mole. At

the same time, the δr parameter suggests the presence of only solid solution phases in HEAs for which $\delta r < 3\%$. Yang and Zhang [14] introduced a thermodynamic parameter $\Omega = T_m \Delta S_{mix}/|\Delta H_{mix}|$ and used it in conjunction with δr to predict phase compositions of HEAs. Here $T_m = \sum c_i T_{mi}$ and T_{mi} is the melting temperature of element. Only solid solution phases were found to form in many HEAs when the conditions $\Omega \geqslant 1.1$ and $\delta r \leqslant 6.6\%$ are met. At the same time, many other HEAs with $1.1 < \Omega < 10$ and $\delta r > 3.8\%$ consist of both solid solution and intermetallic phases, or intermetallic phases only [14]. These observations suggest that intermetallic phases do not form in HEAs in which $\delta r < 3.8\%$ and $\Omega \geqslant 1.1$. The effects of the electronegativity difference, $\delta_\chi = 100\%\sqrt{\sum c_i(1 - \chi_i/\bar{\chi})^2}$, and valence electron concentration difference, $\delta_{VEC} = 100\%\sqrt{\sum c_i(1 - VEC_i/\overline{VEC})^2}$, of the alloying elements on the formation of solid solution phases were studied in works [15,27] and [27], respectively. Here χ_i and VEC_i are the Pauling electronegativity and valence electron concentration, respectively, of element i, $\bar{\chi} = \sum c_i \chi_i$ and $\overline{VEC} = \sum c_i VEC_i$ are the average electronegativity and valence electron concentration of the alloy. No direct correlations between the values of δ_χ and δ_{VEC} and formation of solid solution or intermetallic phases were found. Finally, the average valence electron concentration, VEC, was successfully used by Guo et al. [16] to predict the composition ranges of formation of BCC and FCC solid solution phases in as-solidified $Al_xCoCrCuFeNi$ and $Al_xCoCrFeNi_2$ alloy systems and by Tsai et al. [28] to predict formation of the σ phase in heat treated alloys containing elements of VB to VIIIB groups. Statistical analysis by Guo et al. led to the conclusion that the FCC phases form in HEAs with VEC > 8, BCC phases form at VEC < 6.87 and both FCC and BCC phases coexist in the alloys with VEC values between 6.87 and 8.0 [16]. At the same time, Tsai et al. revealed that the HEAs having VEC values between 6.88 and 7.84 are prone to σ phase formation either in the as-solidified state or during aging at suitable temperatures [28]. It was however noticed that the presence of Cu (and refractory elements) makes this criterion unreliable. A conflict can also be seen between the two above-mentioned criteria for HEAs with VEC values between 6.88 and 7.88, as Guo et al. predict the presence of two-phase, FCC + BCC, structure, while Tsai et al. predict formation of the σ phase in this VEC region. Thus, additional criteria are required to justify the formation of the σ phase in HEAs.

In the present work, the above-mentioned parameters were calculated for the studied HEAs alloys in order to verify if these parameters correlate with the formation of the observed phases. The atomic radius, r_i, electronegativity, χ_i, valence electron concentration, VEC_i, melting temperature, T_{mi}, of the constitutive pure elements, as well as their crystal structure, are given in Table 7. The calculated δr, $\delta \chi$, δVEC, VEC, ΔH_{mix}, ΔS_{mix}, and Ω parameters are given in Table 8. Analysis of the data, given in Table 7 shows that (i) in all four studied alloys, at least 3 alloying elements have different crystal lattices and thus formation of continuous solid solutions should be restricted by one of Hume-Rothery rules [12,25], and (ii) considering other parameters (atomic radii, electronegativity, and VEC), Co, Fe and Ni can be treated as very similar elements, whereas Cr, Mn and V are different from the 3 above-mentioned elements.

Analysis of the data shown in Table 8 reveals that all the alloys satisfy the conditions $\Omega \geqslant 1.1$ and $\delta_r \leqslant 6.6\%$ for the formation of solid solutions. All four alloys have $\delta_r \leqslant 3.0\%$, which should restrict formation of intermetallic phases. However, only the first two alloys are single-phase solid solutions. It is likely that the Ω criterion is valid for the prediction of the formation of solid solution phases at temperatures just below the melting temperature or for rapidly quenched alloys. With a decrease in temperature the entropy term, $T\Delta S_{mix}$, decreases resulting in an increase in the Gibbs free energy

Table 7
Atomic radius, shear modulus, electronegativity, vacancy electron concentration, and melting temperature of the constituent elements of the studied alloys [29].

Element	Co	Cr	Fe	Ni	Mn	V
Atomic radius, pm	125	128	126	124	127	134
Shear Modulus, GPa	75	115	82	76	81	47
Pauling Electronegativity	1.88	1.66	1.83	1.91	1.55	1.63
VEC	9	6	8	10	7	5
T_m, K	1768	2180	1811	1728	1519	2183
Crystal structure	FCC ($T > 422$ °C), Hexagonal ($T < 422$ °C)	BCC	BCC ($T > 1394$ °C), FCC (911 °C $< T < 1394$ °C), BCC ($T < 911$ °C)	FCC	BCC ($T > 1138$ °C), FCC (1087 °C $< T < 1139$ °C), Complex Cubic ($T < 1138$ °C)	BCC

Table 8
Calculated parameters δr, ΔH_{mix}, ΔS_{mix}, ΩVEC, $\delta \chi$, and δVEC for studied alloys.

Alloy	δr, %	ΔH_{mix}, kJ/mole	ΔS_{mix}, J/mole K	Ω	VEC	$\delta\chi$, %	δVEC, %
CoCrFeNi	1.2	−3.75	11.53	5.75	8.25	5.3	17.9
CoCrFeNiMn	1.1	−4.16	13.38	5.79	8.00	7.8	17.7
CoCrFeNiV	2.8	−8.96	13.38	2.89	7.60	6.5	24.4
CoCrFeNiMnV	2.6	−7.5	14.9	3.70	7.50	7.8	22.8

of the solid solution and a decrease in the ratio $T\Delta S_{mix}/|\Delta H_{mix}|$. The FCC solid solutions in the CoCrFeNi and CoCrFeNiMn alloys and the presence of the σ phase in the V-containing CoCrFeNiV and CoCrFeNiMnV alloys are perfectly predicted by the VEC parameter. Indeed, the VEC values of the CoCrFeNi and CoCrFeNiMn alloys (8.25 and 8.0) satisfy the $VEC \geqslant 8.0$ condition for the formation of the FCC solid solutions [16], while the VEC values of the CoCrFeNiV and CoCrFeNiMnV alloys (7.6 and 7.5, respectively) fall in the range of $6.88 \leqslant VEC \leqslant 7.84$ for the σ-phase formation [28]; although the last two alloys also fall in the range of $6.87 \leqslant VEC \leqslant 8.0$ for the formation of the mixture of the BCC and FCC phases [16]. At the same time, table 8 shows no correlation between the electronegativity difference of the alloying elements and the type of phases formed during solidification, similar to previous studies [15,27].

It is interesting to note that the solid-solution alloys, CoCrFeNi and CoCrFeNiMn, have the smallest values of δr (1.1–1.2%) and δVEC (17.7–17.9%), as well the smallest absolute values of ΔH_{mix} and highest values of Ω, among the studied alloys (see Table 8). This may indicate that formation and preservation down to room temperature of solid solution phases is encouraged in the alloys with small differences in the radii and valence electron concentrations of the alloying elements. Almost twice higher negative values of ΔH_{mix} and, respectively, lower values of Ω are indications of stronger bonding between the alloying elements in the V-containing alloys, which encourages formation of intermetallic phases. Although the compositional dependence of these parameters, averaged over the whole alloy, shows correct tendency (e.g. the stability of the solid solution phases increases with a decrease in δr, δVEC, $|\Delta H_{mix}|$ and an increase in Ω the critical values of these parameters for the formation of intermetallic phases are quite different from those defined in previous work [13,14]. It implies the need for some other approaches to characterize the stability of solid solution phases in HEAs as a function of the alloy composition. In this work, two approaches proposed by Senkov and Miracle [30,31] and Senkov et al. [32] are used to predict the compositional instability of a solid solution phase in high entropy alloys.

In their earlier work, Miracle and Senkov [30,31] have analyzed topological instability of FCC solid solution caused by internal strains on solute atoms. The solid solution crystal lattice is destabilized when solute elements produce local distortions in interatomic spacing and in shear modulus, which are sufficient to change local coordination numbers. The critical relative expansion (or contraction) of the interatomic spacing leading to a change in the coordination number near a solute atom has been calculated

as $|\delta r_c| = 3.8\%$ [30]. The local distortion on element i in the FCC crystal lattice is estimated in accord to method proposed in [32]. Every element in this lattice has 12 nearest-neighbor atoms, thus forming a 13-atom cluster. The local environment around an alloying element i can roughly be estimated if the local composition is assumed to be equal to the average composition of the alloy. Thus, an i element has $N_j = 13c_j$ of j-atom neighbors and $N_i = 13c_i - 1$ of i -atom neighbors ($j \neq i$). Then the lattice, δr_i, and shear modulus, δG_i, distortions (per atom pair) in the vicinity of element i are estimated as an average of the atomic size difference, $\delta r_{ij} = 2(r_i - r_j)/(r_i + r_j)$, and shear modulus difference, $\delta G_{ij} = 2(G_i - G_j)/(G_i + G_j)$, respectively, of this element with its neighbors:

$$\delta r_i = \frac{13}{12} \sum c_j \delta r_{ij} \qquad (1)$$

$$\delta G_i = \frac{13}{12} \sum c_j \delta G_{ij} \qquad (2)$$

The calculated values of δr_i and δG_i near different elements in the studied alloys are given in Table 9. The data given in Table 9 shows very low values of $|\delta r_i|$ in the solid solution alloys, CoCrFeNi and CoCrFeNiMn. $|\delta r_i|$ values in these alloys do not exceed 1.9% and thus are much below the critical value of 3.8% [30]. When V is added to these alloys, the $|\delta r_i|$ values noticeably increase near Co, Fe and Ni atoms and decrease near Cr and Mn atoms (see Table 8), although they do not exceed the critical distortion value $|\delta r_c| = 3.8\%$. At the same time, the lattice distortions at the V atoms are high, 5.5% and 5.6% in the CoCrFeNiV and CoCrFeNiMnV alloys, respectively. These V-induced lattice distortions exceed the critical distortion value required to destabilize the FCC crystal lattice, thus predicting transformation of the FCC solid solution into another phase in these two alloys. Unfortunately, while predicting the topological instability of the FCC solid solution phase, this criterion does not predict which phase or phases would form instead. One can however suggest that this criterion increases probability of formation of the σ phase in HEAs with VEC values falling in the range of 6.88–7.84 [28].

The atom-localized shear modulus distortions in the FCC solid solution are also sensitive to the alloy compositions (Table 9). In the CoCrFeNi and CoCrFeNiMn solid solution alloys δG_i have maximum values near Cr atoms ($\delta G_{Cr} = 0.315$ and 0.327, respectively) and have minimum absolute values (~ 0.034–0.047) near Fe and Mn atoms. The maximum shear modulus distortions in these alloys are observed between the nearest Co and Cr atoms:

Table 9

Calculated lattice, δr_i, and shear modulus, δG_i, distortions near an individual constituent element i in apparent FCC solid solution compositions corresponding to the compositions of the studied alloys.

Alloy		Co	Cr	Fe	Ni	Mn	V
CoCrFeNi	δr_i	−0.006	0.019	0.002	−0.015	–	–
	δG_i	−0.142	0.315	−0.046	−0.128	–	–
CoCrFeNiMn	δr_i	−0.009	0.017	0.000	−0.017	−0.009	–
	δG_i	−0.130	0.327	−0.034	−0.116	−0.047	
CoCrFeNiV	δr_i	−0.020	−0.005	−0.012	−0.029	–	0.055
	δG_i	−0.014	0.434	0.081	0.000	–	−0.501
CoCrFeNiMnV	δr_i	−0.020	0.006	−0.011	−0.028	−0.002	0.056
	δG_i	−0.026	0.424	0.070	−0.011	0.056	−0.513

$\delta G_{Cr-Co} = 0.421$. When vanadium is added, δG_i noticeably increase near Cr and Fe atoms and decrease near Co and Ni atoms, and high distortions of the shear modulus are developed near V atoms in the produced CoCrFeNiV and CoCrFeNiMnV alloys ($\delta G_V = -0.501$ and -0.513, respectively). The maximum shear modulus distortions in these V-containing imaginary solid solutions are observed between the nearest Cr and V atoms: $\delta G_{Cr-V} = 0.840$. Large shear modulus fluctuations are thought to destabilize the FCC solid solutions in the V containing alloys. Instead, the σ phase, in which Cr and V share the same sites [33] and thus avoid (or minimize) their neighboring and reduce shear modulus distortions, forms in these alloys.

The σ phase is frequently observed in HEAs [6,11,23,28], even as the matrix phase [34]. Both of the studied CoCrFeNiV and CoCrFeNiMnV alloys are expected to contain σ phase in accordance with VEC criterion proposed by Tsai [28], however, this criterion does not give the explanation why σ phase is formed. It is well established that σ phase also forms in a number of binary alloy systems, including such systems as Cr–Co, Cr–Fe, Cr–Mn and V–Co, V–Fe, V–Mn and V–Ni [33]. It should be also noted that, according to binary phase diagrams, Cr and V demonstrate unlimited solubility in the solid state [35]. One can therefore suggest that Cr and V share the same sites in the σ phase lattice of the CoCrFeNiV and CoCrFeNiMnV alloys. Formation of the σ phase with complex composition is often reported for different steels [36]. In CoCrFeNiV alloy, the σ phase contains about 46–47% of Cr and V totally. This amount is reasonably close to overlap the homogeneity ranges of the σ phase in corresponding binary systems: about 45–50% Cr for Cr–Fe, about 50–65% Cr for Cr–Co, about 30–65% of V for V–Fe, about 45–70% of V for V–Fe, and 55–75% for V–Ni system [33]. In the CoCoFeNiMnV alloy the content of Cr and V in the σ phase is somewhat lower, about 38%. It correlates well with a lower homogeneity range of the σ phase in Cr–Mn and V–Mn binary systems, i.e. 20–25% of Cr and 10–27% of V, respectively [33]. One can therefore conclude that simultaneous additions of Cr and V to the studied HEAs, together with the previously discussed tendency for the V-induced destabilization of the FCC solid solution, make it possible to form the stable σ phase as one of the constitutive phases in the CoCeFeNiV and CoCeFeNiMnV alloys.

4.3. Relationship between the microstructure and mechanical properties in CoCrFeNiMn$_x$V$_y$ alloys

The tensile testing results of the CoCrFeNi and CoCrFeNiMn alloys reported in this work are in good agreement with previously reported properties [5,6]. Both alloys demonstrate very high ductility during tensile and compressive testing at room temperature. Very good ductility is likely caused by their single-phase FCC solid solution structure. The yield strength of the CoCrFeNiMn alloy ($\sigma_{0.2} = 215$ MPa in as-solidified state and $\sigma_{0.2} = 162$ MPa after annealing) is slightly higher than that of the CoCrFeNi alloy ($\sigma_{0.2} = 140$ MPa and $\sigma_{0.2} = 130$ MPa, respectively), but ductility shows opposite behavior ($\delta = 68\%$ in as-solidified state and $\delta = 71\%$ after annealing in the CoCrFeNiMn alloy and $\delta = 83\%$ and $\delta = 87\%$ in the CoCrFeNi alloy). Higher strength of the Mn-containing alloy has also been reported by Gali and George [5] and this is possibly related with strengthening effect from Mn due to more complex interactions of atoms in the 5-element solid solution. In accord to [32], these stresses are proportional to deviations of atomic radii δr_i and deviations of shear modulus δG_i. Considering data given in Table 9, it can be seen that Mn brings very low deviations of atomic radii and shear modulus, and the strongest obstacles in these alloys are Cr atoms. Therefore, no strengthening of the CoCrFeNi alloy should be expected from the addition of Mn. Different grain size and different grain boundary composition environment may also affect the strength of the alloys; however, the limited set of the experimental data produced for these alloys does not allow us to make any statements on this issue.

Annealing causes some decrease in the strength of both CoCrFeNi and CoCrFeNiMn alloys, which is most probably associated with more homogeneous distributions of the alloying elements in the homogenized alloys. Indirect proof of the role of the chemical homogenization can be found in the fact that the change of mechanical characteristics due to annealing is more pronounced in the CoCrFeNiMn alloy, which has a dendritic structure in the as-solidified condition. $\sigma_{0.2}$ decreases from 215 MPa in the as-solidified state to 162 MPa after annealing in this alloy. A significant decrease in the yield strength is thus associated with the elimination of dendritic segregations upon annealing. The results of compressive and tensile testing of the annealed CoCrFeNi alloy show noticeably higher yield strength obtained in compression ($\sigma_{0.2} = 190$ MPa) versus tension ($\sigma_{0.2} = 130$ MPa), while the tension and compression ductility is comparable: $\delta = 68\%$ and $\varepsilon > 75\%$, respectively. The higher yield strength in compression than in tension was also observed earlier in the CoCrCuFeNiAl$_{0.5}$ HEA, which was primary FCC solid solution [37]. Since in both cases the compression specimens had larger cross-section than the tensile specimens, the difference in the strength during compression and tension can be related to crystallographic texture. However, this can also be an intrinsic feature of HEAs, similar to some conventional and nanocrystalline FCC materials [38]. More detailed study is required to understand the mechanism of the tensile-compression asymmetric behavior of these alloys.

Microhardness of the alloys showcases similar tendencies to strength: it is higher in the CoCrFeNiMn alloy (170HV in as-solidified state and 136HV after annealing) than in the CoCrFeNi alloy (140 HV and 134 HV respectively), annealing results in a decrease in microhardness which is more pronounced in the CoCrFeNiMn alloy.

Addition of V results in the formation of a matrix σ phase with FCC particles inside the matrix and in increases in microhardness of the alloys in more than 3 times, to values in the range of 524–650 HV. A similar hardening effect from the σ phase was reported for the aged Al$_{0.3}$CrFe$_{1.5}$MnNi alloy [33]. The microhardness of the

CoCrFeNiV alloy (~524–587 HV) is somewhat lower than that of the CoCrFeNiMnV alloy (636–650 HV). The effect of annealing on the properties of the CoCrFeNiV and CoCrFeNoMnV alloys is also diverse – it causes significant hardening of the CoCrFeNiV alloy (microhardness increases from 524 HV to 587 HV) but a slight decrease in hardness (from 650 HV to 636 HV) of the CoCrFeNoMnV alloy. The V-containing alloys are composed from two phases with distinctively different mechanical properties – the FCC solid solution, which is soft and ductile, and the tetragonal σ phase, which is hard and brittle [39]. Measurements of the microhardness of the σ phase in homogenized state of the CoCrFeNiV and CoCrFeNiMnV alloys in comparison with hardness of FCC solid solution of the CoCrFeNi and CoCrFeNiMn alloys confirms their difference – FCC phase (134–135 HV) about 7.5 times softer than σ phase (1002 HV in the CoCrFeNiV alloy and 1025 HV in the CoCrFeNiMnV alloy). In such "composite" materials mechanical properties usually follow rule of mixtures, i.e. are determined as the volume-fraction averaged properties of individual phases. In the homogenized state, the volume fraction of the FCC phase is 41% and 27% in the CoCrFeNiV and CoCrFeNiMnV alloys, respectively. Using the rule of mixtures and the microhardness values of the σ- and FCC phases, microhardness of the CoCrFeNiV and CoCrFeNiMnV alloys is estimated as 628 HV and 784 HV, respectively. These values are higher than the experimentally observed ones of 587 HV and 636 HV by 8% and 19%, respectively, but still reasonably close. This analysis indicates that microhardness of the V-containing alloys is proportional to the volume fraction of the σ phase and thus higher microhardness of the CoCrFeNiMnV alloy in comparison with the CoCrFeNiV alloy is due to increasing volume fraction of the σ phase.

The V-containing alloys are very brittle during tensile testing and also show little ductility during compression testing, especially the CoCrFeNiMnV alloy. The matrix σ phase is known to be very brittle [39], and this behavior is demonstrated by the alloys. At the same time, the compression strength of these alloys is very high, $\sigma_{0.2}$ = 1435 MPa for the CoCeFeNiV alloy and $\sigma_{0.2}$ = 1660 MPa for the CoCrFeNiMnV alloy. The strength of the alloys is also expected to follow the rule of mixture, however, we have not been able to find any data on compressive properties of the stand-alone σ phase (most possible due to its brittleness). However, one can check the validity of the rule of mixtures by comparing calculated values of $\sigma_{0.2}$ of the σ phase in two different alloys which could be easily determined. In these calculations, we have assumed that the strength of the FCC phase is $\sigma_{0.2}$ = 190 MPa, in accord with the value obtained during compression testing of the CoCrFeNi alloy. Using the known volume fractions of the σ and FCC phases and experimental $\sigma_{0.2}$ values for the alloys (Table 6), the calculations have returned $\sigma_{0.2} \approx$ 2300 MPa and $\sigma_{0.2} \approx$ 2200 MPa for the σ phase in the CoCeFeNiV and CoCeFeNiMnV alloys, respectively. These values are very close to each other, as it was expected from the comparison of the microhardness of the σ phase in the alloys. So one could say that the strength of the V-containing alloys also follows the rule of mixtures, and the higher strength of the CoCrFeNiMnV alloy is attributed to the higher volume fraction of the σ phase. Slightly higher ductility of the CoCrFeNiV alloy (ε = 2.5%) in comparison with the CoCrFeNiMnV alloy (ε = 0.5%) is probably associated with a higher volume fraction of the ductile FCC phase. Therefore one can suggest that relative fractions of the σ and FCC phases determine mechanical properties of these alloys. Optimization of the chemical composition and heat treatment conditions are needed to obtain of CoCrFeNiMn$_x$V$_y$ HEAs containing σ-phase precipitates inside an FCC solid solution matrix. Alloys with this type of structure can combine reasonably high strength with sufficient ductility and thus be suitable for potential structural applications. For example, a CoCrFeNiV$_{0.5}$ HEA containing 70% of the FCC phase and 30% of the σ phase is expected to have $\sigma_{0.2}$ = 810 MPa and δ = 10%.

5. Conclusions

(1) The CoCrFeNi and CoCrFeNiMn alloys have a single phase FCC solid solution structure whereas the CoCrFeNiV and CoCrFeNiMnV alloys consist of the tetragonal σ phase matrix and FCC second-phase particles. The phase composition of the alloys is not affected by annealing treatment.

(2) Formation of the two-phase crystal structure in the CoCrFeNiV and CoCrFeNiMnV alloys is attributed to poor compatibility of V with other alloying elements, which causes significant distortions in the solid solution crystal lattice and its transformation to the σ phase.

(3) The mechanical behavior of the studied HEAs is correlated with their phase composition. The solid solution CoCrFeNi and CoCrFeNiMn alloys are soft and extremely ductile whereas the σ-phase rich CoCrFeNiV and CoCrFeNiMnV alloys are hard and strong, but very brittle. Optimization of the volume fractions of the FCC and σ phases through the alloy composition is thought to result in an alloy with good combinations of high strength and good ductility.

References

[1] J.-W. Yeh, S.-K. Chen, S.-J. Lin, J.-Y. Gan, T.-S. Chin, T.-T. Shun, C.-H. Tsau, S.-Y. Chang, Adv. Eng. Mater. 6 (8) (2004) 299–303.
[2] C.-Y. Hsu, J.-W. Yeh, S.-K. Chen, T.-T. Shun, Metall. Mater. Trans. A 35A (2004) 1465–1469.
[3] O.N. Senkov, G.B. Wilks, J.M. Scott, D.B. Miracle, Intermetallics 11 (2011) 698–706.
[4] O.N. Senkov, S.V. Senkova, D.B. Miracle, C. Woodward, Mater. Sci. Eng., A 565 (2013) 51–62.
[5] A. Gali, E.P. George, Intermetallics 39 (2013) 74–78.
[6] F. Otto, A. Dlouhy, C. Somsen, H. Bei, G. Eggeler, E.P. George, Acta Mater. 61 (2013) 5743–5755.
[7] A.V. Kuznetsov, D.G. Shaysultanov, N.D. Stepanov, G.A. Salishchev, O.N. Senkov, Mater. Sci. Eng., A 533 (2012) 107–118.
[8] A.V. Kuznetsov, D.G. Shaysultanov, N.D. Stepanov, G.A. Salishchev, O.N. Senkov, Mater. Sci. Forum 735 (2013) 146–151.
[9] Y.P. Wang, B.S. Li, Z.F. Heng, Adv. Eng. Mater. 11 (8) (2009) 641–644.
[10] S. Singh, N. Wanderka, B.S. Murty, U. Glatzel, J. Banhart, Acta Mater. 59 (2011) 182–190.
[11] F. Otto, Y. Yang, H. Bei, E.P. George, Acta Mater. 61 (2013) 2628–2638.
[12] R.E. Smallman, H.W. Ngan, Physical Metallurgy and Advanced Materials, seventh ed., Elsiever Ltd., 2007.
[13] Y. Zhang, Y.J. Zhou, J.P. Lin, G.L. Chen, P.K. Liaw, Adv. Eng. Mater. 10 (6) (2008) 534–538.
[14] X. Yang, Y. Zhang, Mater. Chem. Phys. 132 (2012) 233–238.
[15] S. Guo, C.T. Liu, Prog. Nat. Sci.: Mater. Int. 21 (2011) 433–446.
[16] S. Guo, C. Ng, J. Lu, C.T. Lu, J. Appl. Phys. 109 (2011) 103505.
[17] O.N. Senkov, G.B. Wilks, D.B. Miracle, C.P. Chuang, P.K. Liaw, Intermetallics 18 (2010) 1758–1765.
[18] H.-P. Chou, Y.-S. Chang, S.-K. Chen, J.-W. Yeh, Mater. Sci. Eng., B 163 (2009) 184–189.
[19] T.-T. Shun, L.-Y. Chang, M.H. Shiu, Mater. Char. 70 (2012) 63–67.
[20] M.S. Lucas, G.B. Wilks, L. Mauger, J.A. Munoz, O.N. Senkov, E. Michel, J. Horwath, S.L. Semiatin, M.B. Stone, D.L. Abernathy, E. Karapetova, Appl. Phys. Lett. 100 (2012) 251907.
[21] A. Manzoni, H. Daoud, R. Volkl, U. Glatzel, N. Wanderka, Ultramicroscopy (2013) <http://dx.doi.org/10.1016/j.ultramic.2012.12.015>.
[22] B. Cantor, I.T.H. Chang, P. Knight, A.J.B. Vincent, Mater. Sci. Eng., A 375–377 (2004) 213–218.
[23] M.-R. Chen, S.-J. Lin, J.-W. Yeh, S.-K. Chen, Y.-S. Huang, M.-H. Chuang, Metall. Mater. Trans. A 37A (2006) 1363–1369.
[24] M. Martins, L.C. Casteletti, Mater. Char. 60 (2009) 792–795.
[25] W. Hume-Rothery, The Structure of Metals and Alloys, 1st ed., Institute of Metals, London, UK, 1936.
[26] A. Takeuchi, A. Inoue, Intermetallics 18 (2010) 1779–1789.
[27] O.N. Senkov, S.V. Senkova, C. Woodward, Acta Materialia, 2013 (submitted for publication).

[28] M.-H. Tsai, K.-Y. Tsai, C.-W. Tsai, C. Lee, C.-C. Juan, J.-W. Yeh, Mater. Res. Lett. (2013) <http://dx.doi.org/10.1080/21663831.2013.831382>.

[29] http://en.wikipedia.org/wiki/Atomic_radii_of_the_elements_(data_page); http://en.wikipedia.org/wiki/Electronegativity; http://en.wikipedia.org/wiki/Valence_(chemistry); http://en.wikipedia.org/wiki/Melting_points_of_the_elements_(data_page); http://en.wikipedia.org/wiki/Elastic_properties_of_the_elements_(data_page).

[30] O.N. Senkov, D.B. Miracle, J. Non-Cryst. Solids 317 (2003) 34–39.

[31] D.B. Miracle, O.N. Senkov, Mater. Sci. Eng., A 347 (2003) 50–58.

[32] O.N. Senkov, J.M. Scott, S.V. Senkova, S.V. Miracle, C.F. Woodward, Intermetallics 509 (2011) 6043–6048.

[33] C.F. Joubert, Prog. Mater Sci. 53 (2008) 528–583.

[34] M.-H. Tsai, H. Yuan, G. Cheng, W. Xu, W.W. Jian, M.-H. Chuang, C.-C. Juan, S.-J. Lin, Y. Zhu, Intermetallics 33 (2013) 81–86.

[35] H. Baker, ASM Handbook, vol. 3: Alloys phase diagram, ASM International, USA, 1992.

[36] ASM Handbook, vol. 1: Properties and Selection: Irons, Steels, and High Performance Alloys. ASM International, USA, 1992.

[37] F. Wang, Y. Zhang, G. Chen, H.A. Davies, Int. J. Mod. Phys. B 23 (6&7) (2009) 1254–1259.

[38] A.C. Lund, T.G. Nieh, C.A. Schuh, Phys. Rev. B 69 (2004). 012101/4.

[39] E.O. Hall, S.H. Algie, Int. Mater. Rev. 11 (1) (1966) 61–88.